

Contact Damage in Plasma-Sprayed Alumina-Based Coatings

Antonia Pajares,* Lanhua Wei,[†] and Brian R. Lawn^{*}Materials Science and Engineering Laboratory, National Institute of Standards and Technology,
Gaithersburg, Maryland 20899Christopher C. Berndt^{*}Department of Materials Science and Engineering, State University of New York at Stony Brook,
Stony Brook, New York 11794

A study of Hertzian contact damage in plasma-sprayed alumina-based ceramic coatings on steel substrates has been made. Presectioned specimens are used to identify subsurface micromechanical damage processes within the coating and substrate layers as a function of increasing contact load, from both postcontact and *in situ* observations. Damage occurs principally by cracking in the ceramic coating and plastic deformation in the metal substrate, along with delamination at the coating/substrate interface. Coating thickness, cycling loading (fatigue), and processing history (coating microstructure) are shown to be important factors in the damage patterns and ensuing modes of failure. Indentation stress-strain curves are used to measure macroscopic mechanical responses, to quantify the maximum sustainable contact stresses and to determine the relative roles of coating and substrate in the net deformation.

I. Introduction

PLASMA-SPRAYED ceramic coatings up to several hundred micrometers thick are used on metal surfaces to confer wear and erosion resistance, corrosion protection, and thermal or electrical insulation.¹⁻⁴ Such coatings have a tendency to be highly defective in their microstructures, with pores, laminar microcracks, and unmolten phases. They consequently are subject to severe mechanical degradation from concentrated mechanical and thermal stresses, especially in repetitive loading. Yet these same coatings are sufficiently damage tolerant that they can attain more than adequate lifetimes in many practical applications.⁴

Despite this practical success, few studies have been aimed at systematic analysis of damage modes in terms of basic materials and geometrical properties. Well-defined materials-evaluation protocols for plasma-spray and other brittle coating systems appear to be desirable. For instance, it is recognized that the lifetimes of coating systems are sensitive to many factors. Among these factors are number of loading cycles, coating thickness, and processing variables such as starting powder composition and deposition history that influence the microstructure. This raises a vital question: what are the best combinations of such factors for optimum resistance to damage accumulation?

Accordingly, in the present paper Hertzian contact damage in plasma-sprayed alumina-based coatings on soft steel substrates

is studied. The Hertzian test uses spherical indenters to introduce damage in a controlled manner. It is simple yet powerful and has direct relevance to damage accumulation and fatigue wear resistance in bearing stress fields. Originally used to analyze cone fractures in ideally homogeneous brittle solids,⁵⁻⁸ the Hertzian test has recently been applied to the study of subsurface quasi-plastic damage in tough ceramics with heterogeneous microstructures (i.e., weak internal boundaries, large and elongate grains, and high internal stresses).⁹⁻¹⁵ Adaptation to ceramic layer systems is even more recent.¹⁶⁻¹⁸ In the present paper this adaptation is extended to the exploration of coating thickness, cyclic loading, and microstructural change as elements in the underlying stress-strain behavior of a model plasma-spray ceramic coating system. For the coating, alumina-titania ($\text{Al}_2\text{O}_3\text{-TiO}_2$) is chosen because it is relatively easy to produce in a uniform state; however, some "pure," but defective, alumina (Al_2O_3) coatings are also included for comparison. Characterization of the damage in the coating/substrate specimens is achieved primarily by optical microscopy of "bonded-interface" sections using conventional spherical indenters, with ancillary *in situ* tests using cylindrical indenters. Indentation stress-strain curves from the same coating/substrate specimens are used to quantify the damage tolerance and to provide data for future fracture and deformation analyses.

II. Experimental Procedure

(1) Materials Selection and Characterization

Alumina-titania ($\text{Al}_2\text{O}_3\text{-40 wt% TiO}_2$) was selected as a model ceramic coating material. Coatings were air-plasma-sprayed onto grit-blasted soft steel substrates ~3 mm thick. No bond coat was used. The coatings were deposited to average thicknesses of 130–200 μm (designated as "thin" coatings) and 350–500 μm ("thick" coatings) onto the substrates and to ~5 mm in free-standing form.

Sections of cut specimens were diamond-polished to a 1 μm finish for characterization. The microstructure of the plasma-sprayed $\text{Al}_2\text{O}_3\text{-40 wt% TiO}_2$ material is shown in Fig. 1(a). A characteristic lamella splat structure is observed, with compositional variations evident as the wavy texture.¹⁹ Small pores in the structure are associated with processing defects; occasional larger ones are attributed to pull-out of particles during ceramographic preparation. Digital analysis of computer-scanned images indicates a maximum porosity of ~4% in this structure.

Exploratory Vickers tests were performed on polished specimens to obtain a precursory deformation and fracture characterization. Indentation hardness measurements (applied load divided by projected contact area²⁰) yielded 5.0 ± 0.2 GPa for the $\text{Al}_2\text{O}_3\text{-40 wt% TiO}_2$ and 1.2 ± 0.1 GPa for the steel. The coating material is therefore harder than the substrate material but substantially softer than ordinary dense alumina (~18 GPa). Cracks from the indentation corners in free-standing $\text{Al}_2\text{O}_3\text{-40 wt% TiO}_2$ sections were macroscopically well-

R. H. Dauskardt—contributing editor

Manuscript No. 192304. Received September 25, 1995; approved January 23, 1996. Supported by the U.S. Air Force Office of Scientific Research, the National Science Foundation, and the Ministerio de Educación y Ciencia (DGICYT), Madrid, Spain.

*Member, American Ceramic Society.

*Guest Scientist from Departamento de Física, Universidad de Extremadura, 06071-Badajoz, Spain.

*Guest Scientist on leave from Department of Physics and Astronomy, Wayne State University, Detroit, Michigan 48201.

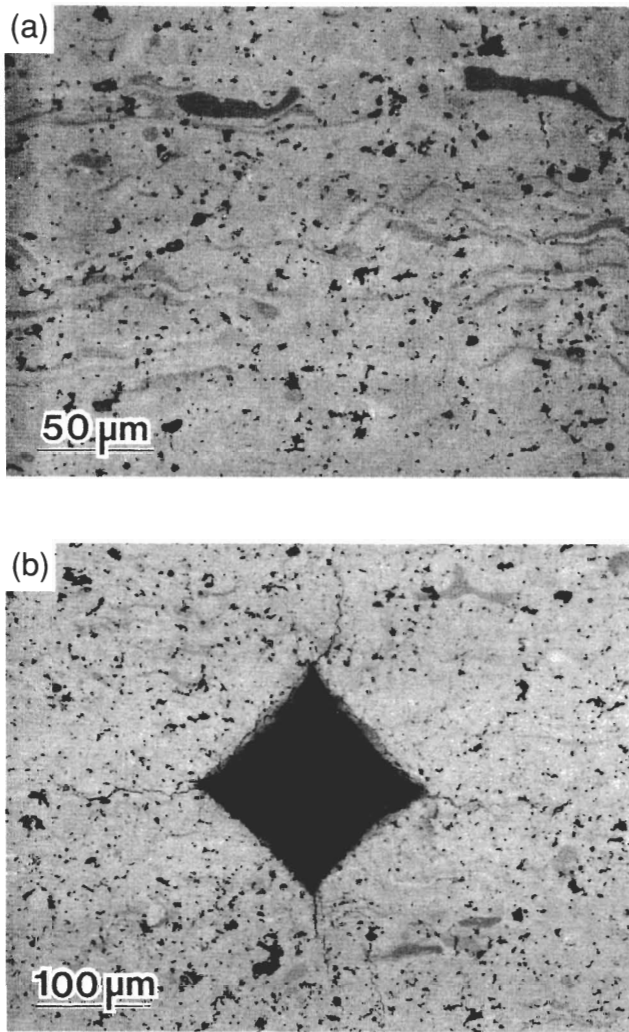


Fig. 1. Optical micrographs, showing section through plasma-sprayed Al_2O_3 -40 wt% TiO_2 ceramic, plasma-spray direction vertical: (a) unindented area, (b) indented area with Vickers diamond pyramid at load 100 N. Wavy microstructure indicates TiO_2 phase. Note porosity. Radial cracks from indentation corners show irregularities at microscopic scale, but are relatively well-formed macroscopically with approximately equal arm lengths.

defined, with radial arms of approximately equal length normal and parallel to the thermal spray direction (Fig. 1(b)). This indicates relative isotropy in the fracture properties, notwithstanding the textured microstructure.

Some pure Al_2O_3 specimens from a previous study¹⁸ are also included in the present work, to demonstrate the influence of processing history. These coatings show a similar microstructure, but with defective layers associated with successive, interrupted torch passes and a porosity of $\sim 8\%$. Such defective layers were meticulously avoided in the processing of the Al_2O_3 -40 wt% TiO_2 specimens.

(2) Hertzian Indentation Tests

Specimens were first prepared for contact testing and subsequent examination of associated subsurface damage patterns. Bars with surface dimensions $25 \text{ mm} \times 3.5 \text{ mm}$ were cut from the coating/substrate composites and free-standing coatings. Cross sections from adjacent cuts were then polished to a $1 \mu\text{m}$ finish and bonded together (Fig. 2) by adhesive, in the case of the free coatings,^{11,12} and by screws through carefully aligned holes in the metal, in the case of the layer composites.¹⁸ The tops of the bonded specimens then were lightly ground and final polished to a $1 \mu\text{m}$ flat finish. Previous studies^{11,12,21} have confirmed that, provided the opposing specimen halves remain

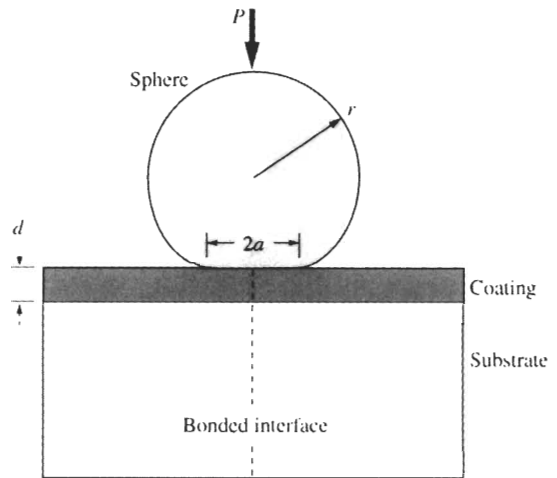


Fig. 2. Schematic of Hertzian test. Sphere of radius r on coating thickness d produces contact of radius a at load P . Some specimens are presectioned to form “bonded interface” for subsurface examination.

in intimate contact during the experiment, potential artifacts in the damage pattern from stress relaxation at the internal interface are easily avoided.

Hertzian tests were then made symmetrically on these top surfaces, along the trace of the bonded interface, in the manner of Fig. 2. The tests were performed in a servohydraulic testing machine (Model 8502, Instron Corp., Canton, MA) using tungsten carbide spheres of radius $r = 3.18 \text{ mm}$ in air. Sequences of single-cycle contacts were made at peak loads, up to $P = 1500 \text{ N}$, with a load/unload time of 0.1 s . Multiple contacts were made at peak loads up to $P = 500 \text{ N}$ and at a frequency of 10 Hz (to match the contact period in single-cycle loading) under sinusoidal load control, over $n = 1$ – 10^5 cycles. After separation, the bars were gold-coated and examined by Nomarski interference microscopy to reveal the subsurface damage.

Some ancillary contact experiments were performed on coating/substrate specimens using a cylinder of radius 1.58 mm in place of the sphere, with the cylinder axis aligned perpendicular to a polished section, to enable *in situ* observation of the damage evolution during a complete load/unload cycle. Results using this configuration were not as definitive as those that were obtained with the spherical indenters, owing to greater difficulty in aligning the indenting cylinder and to a somewhat lower optical resolution. They nevertheless afforded considerable insight into the general sequence of damage events. The specimen cross sections were viewed using a color video camera (Model AS12, Volpi AG, Urdorf/Zürich, Switzerland) with a lens of 50 mm working distance, and the visual images recorded on a video recording machine. These tests were performed slowly on a screw-driven machine (Model 1122, Instron Corp.), in a 5 min load/unload cycle, to follow the damage evolution.

Indentation stress-strain curves^{9,12} were measured on polished top surfaces of coating/substrate composite and free-standing coating and substrate specimens. These surfaces were gold-coated prior to contact, to allow subsequent measurement of residual impressions in the deformed thin metal layer (especially at low loads). Indentations were made with tungsten carbide spheres of radius $r = 1.98$ and 3.18 mm on coating/substrate composites, and $r = 1.98, 3.18, 7.94,$ and 12.7 mm on free-standing forms (the two larger radii in the latter case to extend the data range to lower strains). Loads up to $P = 3000 \text{ N}$ were applied using the screw-driven testing machine. The contact radius a was determined from the residual impression at each indentation⁹ to obtain indentation stress ($P/\pi a^2$) as a function of indentation strain (a/r).

III. Results

(I) Hertzian Damage Characterization

Sequences of subsurface Hertzian contact damage patterns from bonded-interface specimens are shown in Figs. 3, 4, 6, and 7 for a single sphere radius $r = 3.18$ mm. These sequences illustrate the effects of coating thickness, contact load, number of contact cycles, and coating microstructure. Arrows at top of the micrographs indicate contact diameters, $2a$.

(A) *Effect of Coating Thickness:* Figure 3 shows micrographs of single-cycle contact damage in the Al_2O_3 -40 wt% TiO_2 system, for (a) free-standing coating material, (b) thick coating on steel, and (c) thin coating on steel. These tests have been made at a common peak load $P = 1000$ N. In the free-standing coating (Fig. 3(a)), a drop-shaped damage zone of depth $\sim 2a$ is observed in the subsurface region of concentrated shear stress. This drop-shaped damage geometry is characteristic of bulk ceramics with microstructural heterogeneity and high flaw tolerance.^{9,11-15} Higher-magnification examinations show the damage to consist of a high density of discrete and constrained microfailures, preferentially along weak boundaries. No trace of classical cone cracks of the type found in homogeneous, ideally brittle solids⁸ is evident.

In the coating/substrate layer composites (Figs. 3(b) and (c)), the damage pattern is strongly modified by the substrate, with progressive transfer of the "plasticity" to the soft substrate at diminishing coating thickness d . The plasticity in the substrate is apparent as an expanding hemispherical zone, and in the coating in Fig. 3(b) as an ever-constrained "caplike" damage zone immediately beneath the contact.¹⁸ A consequence of the progressive transfer of load to the soft substrate is an attendant expansion of the contact diameter and residual coating depression, although the applied load remains the same in all cases in Fig. 3.

The most conspicuous component of the coating damage in Figs. 3(b) and (c) is the fracture pattern, consisting of downward-extending conelike cracks from the top surface and upward-extending transverse cracks from the lower interface. The cone cracks are axisymmetrical,⁸ and the upward-extending cracks are shallow, near-circular segments contained in axial planes.³ These cracks, once initiated, are highly stable: they are well contained in the thick coating in Fig. 3(b), and approach full penetration only in the thinner coating in Fig. 3(c). Any such penetration will inevitably diminish the load support provided by the coating and further transfer this support to the substrate. Delamination at the coating/substrate interfaces also is apparent in Figs. 3(b) and (c), again more so in the thinner coating. (Recall that there is no bond coat in this system, which otherwise might inhibit separation.¹⁸) Note that the delamination cracks are contained within the diameter of the substrate yield zone.

(B) *Effect of Contact Load:* Figure 4 consists of two series of micrographs, for thick (left) and thin (right) Al_2O_3 -40 wt% TiO_2 coatings on steel, showing the accumulation of single-cycle Hertzian contact damage through loads of $P = 150, 500,$ and 1500 N. The accumulation of damage after the onset of first visible damage is expansive. The location of the first damage is discernible at low load in Figs. 4(a) and (d): in the thick-coating system as subsurface deformation in the coating, immediately beneath the contact; and in the thin-coating system as an incipient plastic zone within the substrate. At intermediate loading (Figs. 4(b) and (e)), damage is observed in the coating and substrate, in both the thick- and thin-coating systems. The first signs of brittle cracking appear, most notably as partially penetrating cone cracks in the thinner coating. Delamination at the coating/substrate interfaces is evident at both thicknesses. At high loading (Figs. 4(c) and (f)), the substrate yield zones extend beyond the contact dimension,

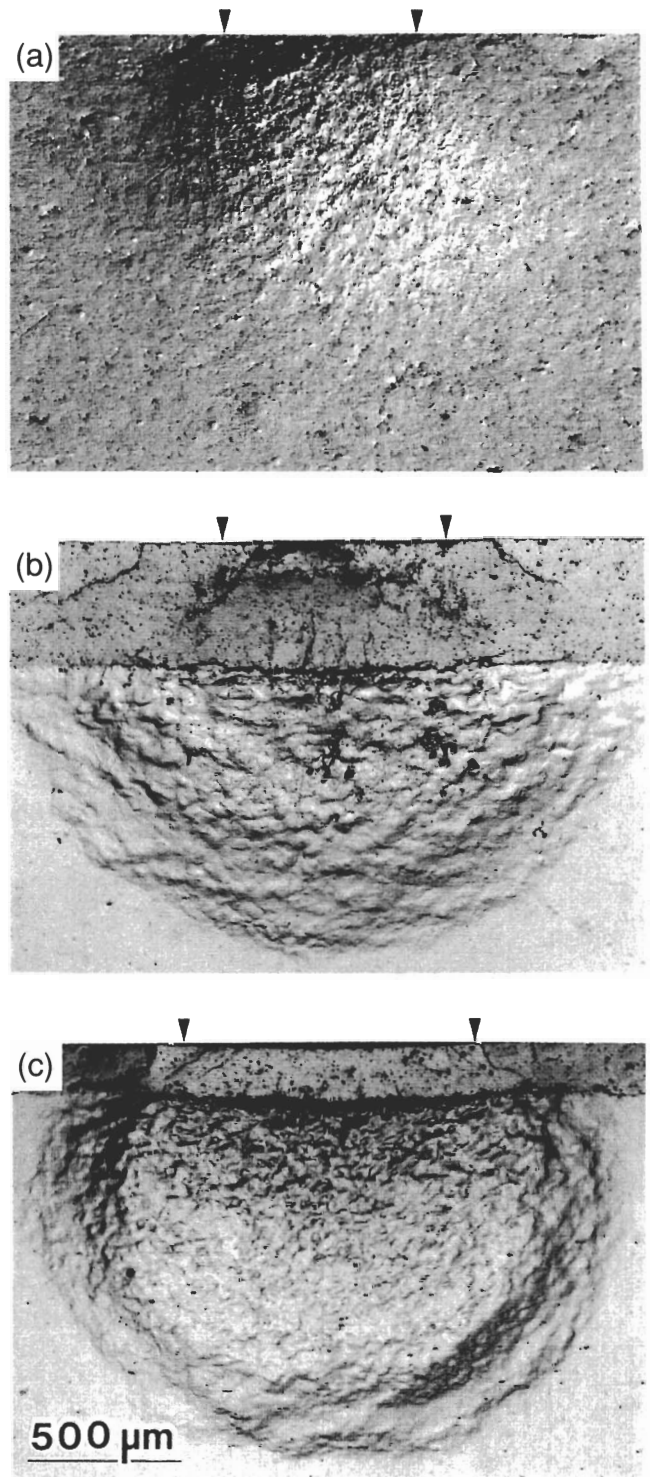


Fig. 3. Optical micrographs (Nomarski illumination) of bonded-interface section of plasma-sprayed Al_2O_3 -40 wt% TiO_2 coatings, showing effect of thickness on Hertzian contact damage: (a) free-standing coating; (b) "thick" coating on steel substrate, $d = 425$ μm ; and (c) "thin" coating on substrate, $d = 170$ μm . Single-cycle indentations made at common sphere radius $r = 3.18$ mm and peak load $P = 1000$ N. Respective contact diameters indicated by arrows correspond to indentation strains $a/r = 0.10, 0.11,$ and 0.15 , respectively.

approaching a state of full plasticity.²⁰ The coatings also indicate through-thickness deformation, with resultant permanent bending. At this point, the coating fracture patterns, including delamination, are well developed, to the extent in the thin-coating system that the conelike cracks appear to have penetrated to the substrate, producing a loose (yet still intact) plug

³This fact is established from direct optical examination of analogous contact damage patterns in bilayer systems in which the coating layer is made of glass.¹⁷

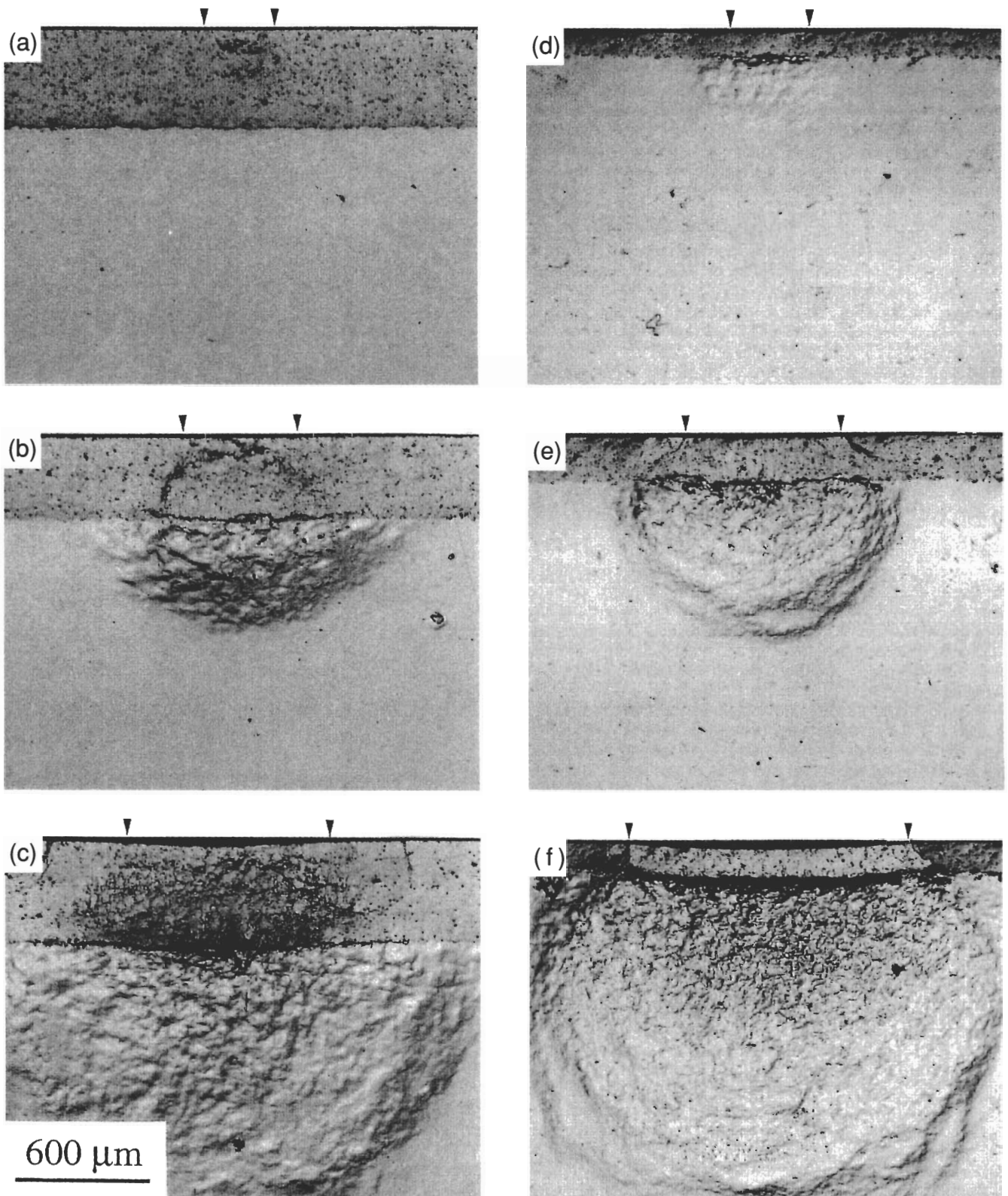


Fig. 4. Optical micrographs (Nomarski illumination) of bonded-interface section of Al_2O_3 -40 wt% TiO_2 sequences for thick (left) and thin (right) plasma-sprayed coatings on steel, showing effect of loading on single-cycle Hertzian contact damage, at sphere radius $r = 3.18$ mm: (a) and (d) $P = 150$ N, (b) and (e) $P = 500$ N, and (c) and (f) $P = 1500$ N. Corresponding indentation strains are indicated in Fig. 8. Contact diameters are indicated by arrows. Note slight differences in thickness within each sequence, reflecting point-by-point and specimen-to-specimen variations in coating conditions.

of material, foreshadowing total failure. In this latter case, the substrate is on the verge of assuming the full brunt of the contact load. Ultimately, at even higher loads, the coatings do indeed fail, by spalling.

The sequence of deformation and fracture initiation and development during the load/unload cycle in Fig. 4 has been

established from the *in situ* observations on thick-coating specimens, notwithstanding the configurational differences associated with the cylindrical indenter. A schematic representation of the damage evolution traced from a video sequence during one loading/unloading cycle on a thick coating is given in Fig. 5. Above a critical level in the loading half-cycle

(Fig. 5(a)), plastic deformation is observed to initiate in the substrate. On further loading (Fig. 5(b)), conelike fractures at the outer top surface and upward-extending cracks at the inner coating/substrate interface are seen to pop in and arrest. On proceeding to peak load (Fig. 5(c)), the substrate yield zone continues to expand and the coating cracks to grow. On unloading (Fig. 5(d)), the latter cracks continue to open and even to propagate, albeit in a highly stable manner. Finally, close to full unload (Fig. 5(e)), the delamination cracks open widely.

(C) *Effect of Number of Cycles:* Micrographs of damage from multiple-cycle contact tests on the Al_2O_3 -40 wt% TiO_2 /steel system are presented in Fig. 6 for thin-coating specimens. The tests are conducted at an intermediate load $P = 500$ N (from Fig. 4(e)), over $n = (a) 1, (b) 10^2,$ and $(c) 10^5$ cycles. There is a small but systematic increase in the substrate plastic zone size with the cycling, attributable to load/unload yield hysteresis.²² The fracture damage in the coating also increases, until at $n = 10^5$ the delamination cracks have opened considerably, and the conelike cracks at the edge of the contact have penetrated to the substrate (cf. damage attained at $P = 1500$ N in Fig. 4(f)).

Thus, the coatings are subject to significant fatigue. Damage, once initiated, accumulates with each cycle, indicating a finite lifetime. Nevertheless, the coating in Fig. 6(c) has not spalled, and should still provide some protection to the substrate.

(D) *Effect of Processing History and Microstructure:* To demonstrate the importance of processing variables, comparative micrographs for Al_2O_3 -40 wt% TiO_2 and Al_2O_3 coating systems are shown in Figs. 7(a) (from Fig. 3(b)) and 7(b), respectively. In these two cases, the tests have been made on thick-coating specimens at a single cycle and a common peak load $P = 1000$ N. There are some similarities in the damage pattern, notably in the substrate yield zone (although not quite as well developed in the Al_2O_3 , consistent with a slightly larger coating thickness), and in the appearance of the caplike distributed deformation in the coating immediately beneath the contact area. This implies some commonality in the yield process in the two Al_2O_3 -based coating materials.

However, there also are some striking differences in the damage patterns, most notably in the form of the coating fracture. In the Al_2O_3 -40 wt% TiO_2 , the cracks are predominantly transverse; in the Al_2O_3 , they are predominantly (but not exclusively) laminar. From *in situ* tests on the latter specimens, these intracoating laminar cracks were observed to form during loading, as initiation of microcracks along the defective interlayers associated with the four interrupted plasma-spray torch passes. The discrete sources coalesced into the macroscopic laminar cracks during unloading. The operation of this alternative fracture mode in the Al_2O_3 appears to have inhibited the development of the transverse fractures. This implies that the mode of coating failure is highly sensitive to the microstructure. Delamination at the coating/substrate interlayer again occurred at the completion of unloading.

(2) Stress-Strain Curves

Indentation stress-strain curves, $p_0(a/r)$, are shown for the Al_2O_3 -40 wt% TiO_2 /steel system in Fig. 8. Data are plotted for free-standing coatings and free-standing substrates, as well as for layer composites of different coating thickness relative to sphere radius, d/r . Solid curves are empirical fits through the data. For the free-standing coatings and free-standing substrates, the stress-strain curves are universally monotonic, independent of r . These curves enable evaluation of two key elastic/plastic parameters:¹⁸ Young's modulus, E , from the initial slopes, in conjunction with the Hertzian elasticity relations, yielding 70 ± 5 GPa (Al_2O_3 -40 wt% TiO_2) and 180 ± 36 GPa (steel); and yield stress, Y , from the contact pressures $p_0 = 1.1Y$ at the onset of plasticity (most accurately determined from presection observations such as Fig. 3(a), made over a range of loads), yielding $Y = 1.9$ GPa (Al_2O_3 -40 wt% TiO_2) and 0.42 GPa (steel). These values of E and Y for Al_2O_3 -40 wt% TiO_2

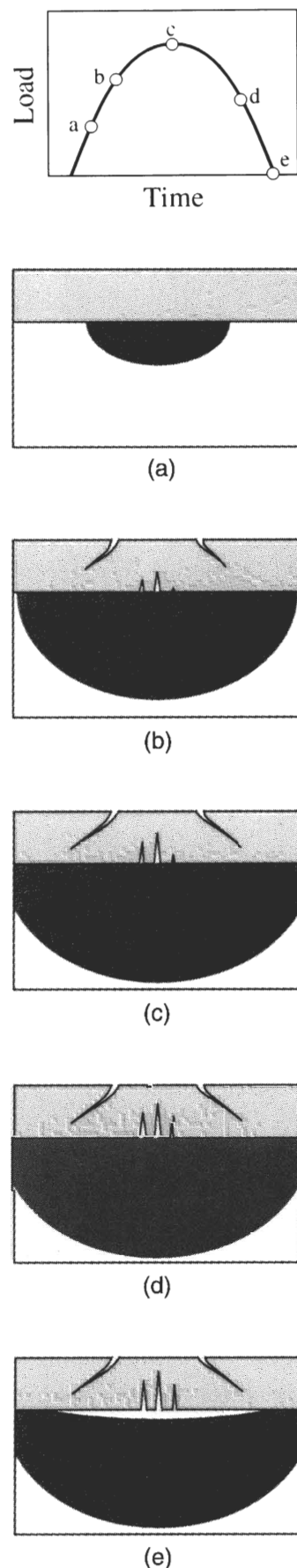


Fig. 5. Evolution of damage in thick plasma-sprayed Al_2O_3 -40 wt% TiO_2 coatings (light shading) on steel. Substrate yield zone (dark shading) and coating fractures traced from *in situ* video recording during load/unload cycle (a)–(e) using cylindrical indenter.

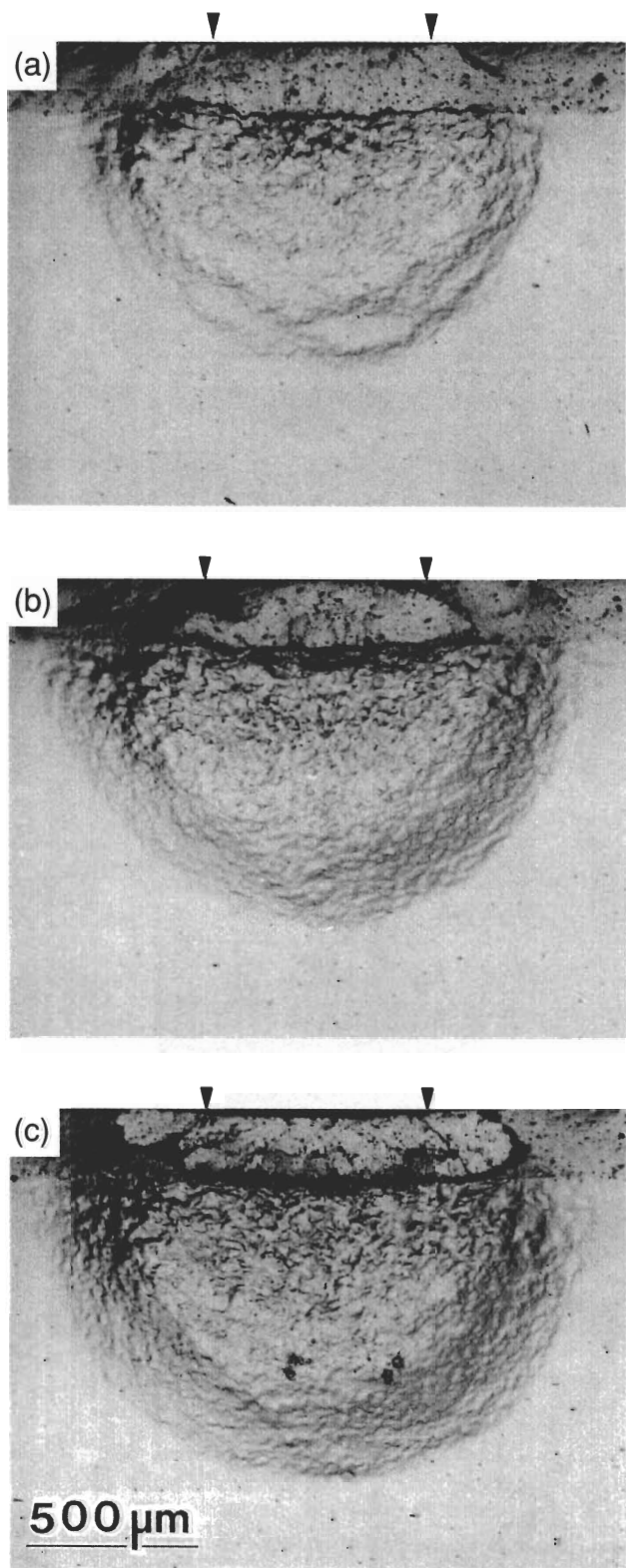


Fig. 6. Optical micrographs (Nomarski illumination) of bonded-interface section of Al_2O_3 -40 wt% TiO_2 for thin plasma-sprayed coatings on steel, showing effect of number of cycles on multiple-cycle Hertzian contact damage, at sphere radius $r = 3.18$ mm and peak load $P = 500$ N: (a) $n = 1$ (from Fig. 4(e)), (b) $n = 10^2$, and (c) $n = 10^5$ cycles. Contact diameters are indicated by arrows.

are within 10% of those obtained previously for Al_2O_3 ,¹⁸ confirming a relative insensitivity of macroscopic stress-strain parameters to composition and microstructure.

For the composite coating/substrate system, $p_0(a/r)$ is no longer a universal function but now depends on d/r , bounded by

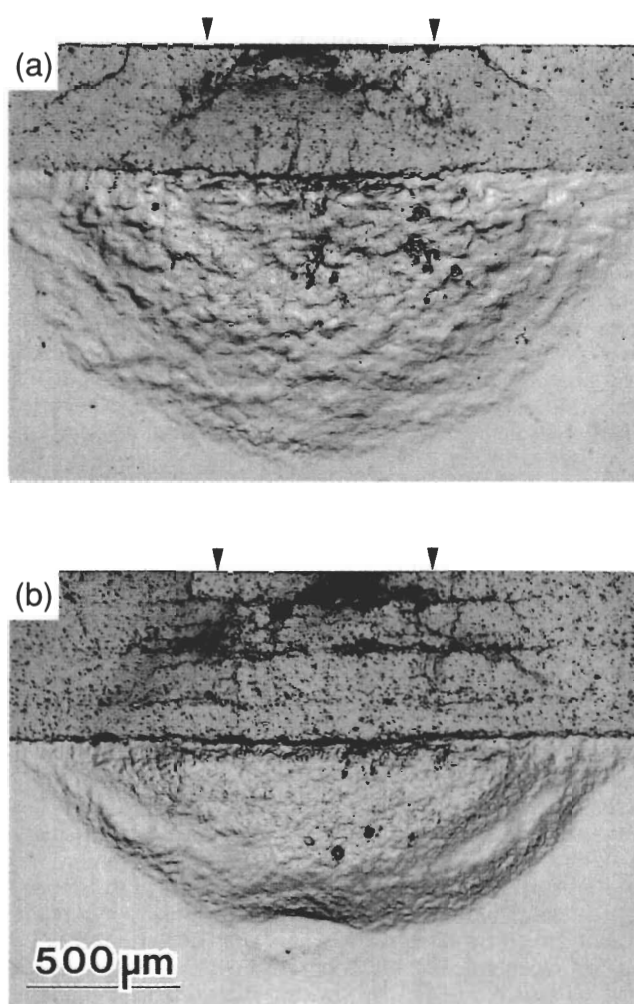


Fig. 7. Optical micrographs (Nomarski illumination) of bonded-interface section of thick plasma-sprayed Al_2O_3 -based coatings, single-cycle damage at sphere radius $r = 3.18$ mm and peak load $P = 1000$ N: (a) Al_2O_3 -40 wt% TiO_2 (from Fig. 3(b)) and (b) Al_2O_3 . Contact diameters are indicated by arrows.

the free-standing coating and substrate curves.¹⁸ With increasing contact load, the coating/substrate data for any given value of d/r initially follow the coating curve closely, but then pass through a maximum, $p_0 = p_m$ say, and finally approach the substrate curve. The implication is that the load is supported elastically by the coating and plastically by the substrate. In this context, it is interesting to refer to the sequences of micrographs for the thick- and thin-coating series in Fig. 4, and to correlate the onset and development of substrate yield with the points "a," "b," and "c" (thick, $d/r = 0.15$) and "d," "e," and "f" (thin, $d/r = 0.050$) marked on the appropriate curves in Fig. 8. Note the comparatively long tail of the thin-coating material in this comparison, indicating an enhanced capacity to absorb strain energy at a given set of contact loading conditions prior to ultimate failure, characteristic of a more damage-tolerant structure.

The maximum in the stress-strain curve warrants additional consideration, because it implies the existence of a limiting sustainable stress for any given coating and contact configuration. Values of p_m are plotted as a function of d/r in Fig. 9, using the determinations for Al_2O_3 -40 wt% TiO_2 from Fig. 8 along with some previous data for Al_2O_3 .¹⁸ Hence, the maximum contact pressure in the alumina/steel coating/substrate system in this experiment increases with either increasing coating thickness at fixed sphere radius or decreasing sphere radius at fixed coating thickness, again somewhat insensitively to the alumina microstructure.

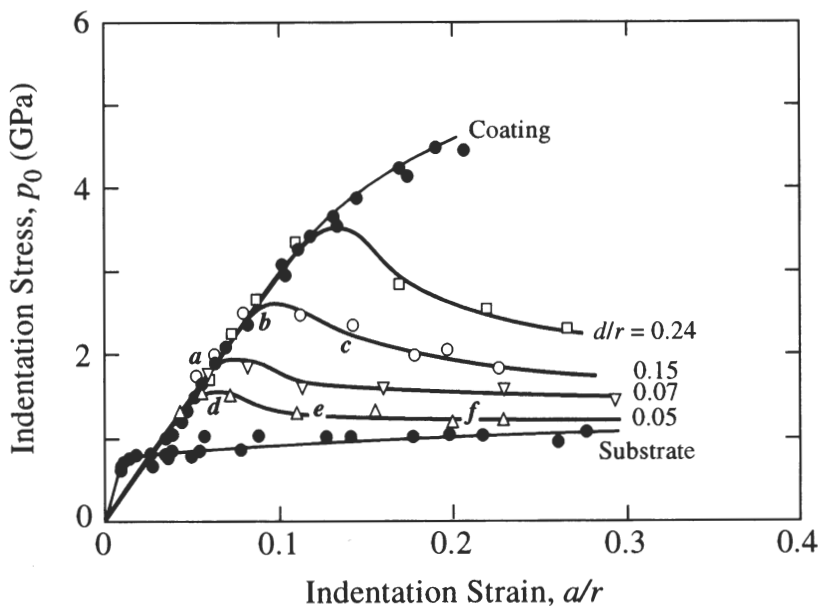


Fig. 8. Indentation stress–strain curves for plasma-sprayed Al_2O_3 –40 wt% TiO_2 coatings on steel. Data for composite coating/substrate systems plotted separately at designated values of coating thickness/sphere radius, d/r , for thick and thin coatings at $r = 1.98$ and 3.18 mm. Data for free-standing coating and substrate plotted for values of $r = 1.98$ – 12.7 mm (not distinguished). Solid curves are empirical fits. Points “a,” “b,” “c,” “d,” “e,” and “f” respectively correspond to micrographs in Fig. 4. Note maximum in curve for each composite coating/substrate system. Beyond tail regions, coatings fail.

IV. Discussion

The results in this study confirm the Hertzian test as a simple but functional means of investigating fracture and deformation modes in ceramic coatings on metal substrates—in this case, plasma-sprayed alumina-based composites on steel—with special relevance to contact problems, bearing stresses, wear and erosion, etc. Specifically, the results confirm the potential of Hertzian testing as a means of evaluating the roles of coating thickness, number of cycles, and microstructural variables in damage accumulation. Even though the Hertzian contact field may not be considered a true representation of many practical stress states (e.g., thermal cycling), it nevertheless constitutes a powerful probe of inherent weaknesses in the structures, without the complexity of simulated rig testing. This kind of macroscopic accumulation of damage in the coating materials is typical of flaw-tolerant ceramics,^{9,23–26} although details of the underlying micromechanisms may be superficially different. Conspicuously, the observations reveal the damage tolerance of

the plasma-spray coatings to be high; even where failure appears imminent, at high load or after many cycles, the coatings continue to afford protection to the substrate. Such observations, in combination with an appropriate stress analysis (see below), would appear to offer a basis for ultimate lifetime predictions of brittle coating systems.

Accordingly, the presectioning technique used to obtain the micrographs in Figs. 3, 4, 6, and 7 reveals the distribution of deformation and fracture damage in both coating and substrate beneath spherical contacts. *In situ* observations using contacts with cylinders (Fig. 5) establish the sequence of the individual damage events. Initially, at low loads, the harder alumina-based coating elastically supports the bulk of the load. Beyond a yield point, quasi-plastic deformation sets in. As the contact zone continues to expand, full plasticity develops in the substrate, which assumes an increasing proportion of the load support. Yield also occurs in the coating, but the main damage there appears as transverse fractures, outer downward-extending conelike cracks and inner upward-extending cracks. These cracks pop in during the loading half-cycle, but continue to evolve in a highly stabilized manner during the unloading half-cycle. Interlayer delamination occurs toward the end of unloading. The presence of an intervening bond coat can help alleviate this delamination.¹⁸

It is instructive to rationalize the damage patterns in terms of combined Hertz and flexure fields. The difference in elastic/plastic properties between the coating and the substrate accounts for the changes in damage mode in Fig. 3 as the coating thickness decreases. Thus, elastic/plastic mismatch redistributes the concentrated shear stresses immediately below the indenter, thereby transferring the yield zone progressively into the soft substrate. The same mismatch redistributes the tensile stresses in the coating during the loading half-cycle, the more so as the coating thickness decreases. The thinner coating layer may be considered to behave more like a constrained flexural plate supported by a still-elastic outer contact boundary and soft plastic underlayer, and less like a purely Hertzian semi-infinite solid. This transition to a greater flexural component inevitably concentrates the tensile coating stresses at the upper free surface shoulders outside the circle of contact and at the coating/substrate interface within the contact, where the transverse cracks develop. At the same time, these flexural stresses

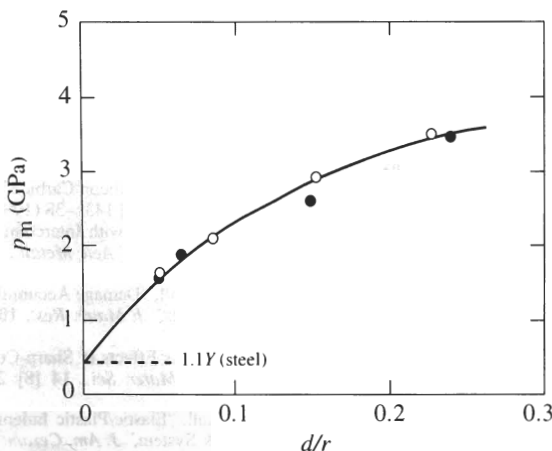


Fig. 9. Plot of maximum stress, p_m , from Fig. 8 and Ref. 18, as function of d/r . Yield stress in metal provides lower limit for zero-thickness coatings (\bullet) Al_2O_3 –40 wt% TiO_2 coatings on steel and (\circ) Al_2O_3 coatings on steel.

must be strongly compressive on the opposing sides of the neutral planes, thus stabilizing the fractures. In making this argument for an increasingly important flexural stress component, the ever-present contribution from the contact field cannot be disregarded, even in the thinnest coatings. The contact field superposes strong elastic compressive stresses onto the transverse cracks, released only when the indenter is withdrawn. Such release explains the continued crack extension during unloading, in the well-documented manner of radial and lateral cracks in residual contact fields beneath Vickers indentations in homogeneous materials,^{27,28} and of shear-fault-induced, grain-localized microcracks beneath Hertzian indenters in heterogeneous materials.²⁹ Perhaps the strongest of all manifestations of elastic/plastic mismatch is the generation of high residual tension at the coating/substrate interface immediately above the substrate plastic zone, where delamination occurs. This extreme mismatch is attributed to a relatively high elastic recovery in the flexed coating layer, again reaching its maximum at complete unload.

To place these observations on a more quantitative footing, and to establish a basis for future fracture-mechanics analysis, a detailed stress analysis is necessary. The invariably complex elastic/plastic fields in the deformed coating structures considered in this paper appear to be beyond analytical solution—numerical evaluation techniques (e.g., finite-element modeling) seem to be necessary. Specifically required are shear-stress distributions in the substrate and coating, to confirm the plastic zone geometry, and tensile stress distributions in the coating, to confirm the fracture geometry. A test of any such stress analysis is self-consistency between the calculated and measured indentation stress-strain curve. The present results establish an environment for such calculations not only by defining the deformation and fracture configurations to be modeled but also by providing essential input parameters, e.g., coating thickness and sphere size, Young's modulus, and yield stress.

The indentation stress-strain curves in Fig. 8 provide a graphical representation of damage evolution in the coating/substrate system. In the present case, where the substrate is considerably softer than the coating, the stress-strain curve exhibits a well-defined maximum, p_m . Prior to the maximum, the strain is governed principally by the properties of the coating; beyond the maximum, the strain is transferred progressively to the substrate. The value of p_m is a measure of the maximum sustainable stress in the composite system. Increasing the thickness of the coating relative to the contact diameter increases p_m (Fig. 9), effectively increasing the hardness of the composite structure. As may be attested by comparison tests on other coating/substrate structures,¹⁸ the very existence of p_m is contingent on the substrate being softer than the coating—the reverse case leads to an ever-increasing monotonic curve. The long strain-softening tail, most pronounced at the lower values of d/r in Fig. 8, indicates a damage-tolerant, energy-absorbing structure. Note, for instance, that the point f for $d/r = 0.050$ extends much farther along the tail than the corresponding point c for $d/r = 0.15$ at the same contact load (recall Fig. 4). Hence damage tolerance is gained at the expense of effective structural hardness. Such competing elements, along with the fracture characteristics described above, could be important considerations in the general design of brittle coatings on soft substrates.

Finally, comment may be made on the influence of microstructure based on the brief comparison in this experiment between Al_2O_3 -40 wt% TiO_2 and Al_2O_3 coatings. Essentially, the effect of microstructural variation from different processing histories is felt only slightly in the elastic/plastic properties, but is crucial in the fracture properties. For the elastic/plastic properties, recall the similarity of E and Y values for these two Al_2O_3 -based materials (Section III(2)), indicating an insensitivity of macroscopic stress-strain response to structural details.¹⁸ The fracture properties, on the other hand, are extremely vulnerable to weaknesses in the structures (Fig. 7). Thus in the

Al_2O_3 , preexistent laminar weaknesses promote intralayer delaminations. These delaminations, by relaxing the stress buildup, most likely suppress the transverse fractures observed in the other, more isotropic Al_2O_3 -40 wt% TiO_2 material. In the context of engineering lifetime, the failure mode and other critical operational properties, such as heat transfer in thermal barrier coatings, may be highly dependent on the microstructural complexion. Interactions between mechanical and thermal properties may constitute a rich area for future study.

Acknowledgments: Thanks are due to G. Bancke for assistance in preparing the coatings, E. R. Fuller for the computer evaluations of porosities in the coating materials, and T.-N. Ying for assistance with the *in situ* experiments.

References

- H. Herman, "Plasma-Sprayed Coatings," *Sci. Am.*, **256** [9] 113–88 (1988).
- H. Herman, "Plasma Spray Deposition Processes," *MRS Bull.*, **13**, 60–67 (1988).
- H. Herman, C. C. Berndt, and H. Wang, "Plasma-Sprayed Ceramic Coatings"; pp. 131–88 in *Ceramic Films and Coatings*. Edited by J. B. Wachtman and R. A. Haber. Noyes, Park Ridge, NJ, 1993.
- L. Pawlowski, *The Science and Engineering of Thermal Spray Coatings*. Wiley, New York, 1995.
- H. Hertz, *Hertz's Miscellaneous Papers*; Chs. 5 and 6. Macmillan, London, U.K., 1896.
- F. C. Roesler, "Brittle Fractures Near Equilibrium," *Proc. Phys. Soc., London, Sect. B*, **69**, 981 (1956).
- F. C. Frank and B. R. Lawn, "On the Theory of Hertzian Fracture," *Proc. R. Soc. London, A*, **299** [1458] 291–306 (1967).
- B. R. Lawn and T. R. Wilshaw, "Indentation Fracture: Principles and Applications," *J. Mater. Sci.*, **10** [6] 1049–81 (1975).
- F. Guiberteau, N. P. Padture, H. Cai, and B. R. Lawn, "Indentation Fatigue: A Simple Cyclic Hertzian Test for Measuring Damage Accumulation in Polycrystalline Ceramics," *Philos. Mag. A*, **68** [5] 1003–16 (1993).
- B. R. Lawn, N. P. Padture, H. Cai, and F. Guiberteau, "Making Ceramics 'Ductile,'" *Science*, **263**, 1114–16 (1994).
- F. Guiberteau, N. P. Padture, and B. R. Lawn, "Effect of Grain Size on Hertzian Contact in Alumina," *J. Am. Ceram. Soc.*, **77** [7] 1825–31 (1994).
- H. Cai, M. A. Stevens Kalceff, and B. R. Lawn, "Deformation and Fracture of Mica-Containing Glass-Ceramics in Hertzian Contacts," *J. Mater. Res.*, **9** [3] 762–70 (1994).
- N. P. Padture and B. R. Lawn, "Toughness Properties of a Silicon Carbide with an *In-Situ*-Induced Heterogeneous Grain Structure," *J. Am. Ceram. Soc.*, **77** [10] 2518–22 (1994).
- H. H. K. Xu, L. Wei, N. P. Padture, B. R. Lawn, and R. L. Yeckley, "Effect of Microstructural Coarsening on Hertzian Contact Damage in Silicon Nitride," *J. Mater. Sci.*, **30**, 869–78 (1995).
- A. Pajares, F. Guiberteau, B. R. Lawn, and S. Lathabai, "Hertzian Contact Damage in Magnesia-Partially-Stabilized Zirconia," *J. Am. Ceram. Soc.*, **78** [4] 1083–86 (1995).
- L. An, H. M. Chan, N. P. Padture, and B. R. Lawn, "Damage-Resistant Alumina-Based Layer Composites," *J. Mater. Res.*, **11** [1] 204–10 (1996).
- S. Wuttiphan, B. R. Lawn, and N. P. Padture, "Crack Suppression in Strongly Bonded Homogeneous/Heterogeneous Laminates: A Study on Glass/Glass-Ceramic Bilayers," *J. Am. Ceram. Soc.*, **79** [3] 634–40 (1996).
- A. Pajares, L. Wei, B. R. Lawn, N. P. Padture, and C. C. Berndt, "Mechanical Characterization of Plasma-Sprayed Ceramic Coatings on Metal Substrates by Contact Testing," *Mater. Sci. Eng., A*, **208** [2] 158–65 (1996).
- J. Ilavsky, "Studies of Plasma Sprayed Alumina"; Ph.D. Thesis. State University of New York at Stony Brook, Stony Brook, NY, 1994.
- D. Tabor, *Hardness of Metals*. Clarendon, Oxford, U.K., 1951.
- T. O. Mulhearn, "The Deformation of Metals by Vickers-Type Pyramidal Indenters," *J. Mech. Phys. Solids*, **7**, 85–96 (1959).
- S. Suresh, *Fatigue of Materials*. Cambridge University Press, Cambridge, U.K., 1991.
- H. Cai, M. A. S. Kalceff, B. M. Hooks, B. R. Lawn, and K. Chyung, "Cyclic Fatigue of a Mica-Containing Glass-Ceramic at Hertzian Contacts," *J. Mater. Res.*, **9** [10] 2654–61 (1994).
- N. P. Padture and B. R. Lawn, "Contact Fatigue of a Silicon Carbide with a Heterogeneous Grain Structure," *J. Am. Ceram. Soc.*, **78** [6] 1431–38 (1995).
- N. P. Padture and B. R. Lawn, "Fatigue in Ceramics with Interconnecting Weak Interfaces: A Study Using Cyclic Hertzian Contacts," *Acta Metall.*, **43** [4] 1609–17 (1995).
- A. Pajares, L. Wei, B. R. Lawn, and D. B. Marshall, "Damage Accumulation and Cyclic Fatigue in Mg-PSZ at Hertzian Contacts," *J. Mater. Res.*, **10** [10] 2613–25 (1995).
- D. B. Marshall and B. R. Lawn, "Residual Stress Effects in Sharp-Contact Cracking: I. Indentation Fracture Mechanics," *J. Mater. Sci.*, **14** [8] 2001–12 (1979).
- B. R. Lawn, A. G. Evans, and D. B. Marshall, "Elastic/Plastic Indentation Damage in Ceramics: The Median/Radial Crack System," *J. Am. Ceram. Soc.*, **63** [9–10] 574–81 (1980).
- B. R. Lawn, N. P. Padture, F. Guiberteau, and H. Cai, "A Model for Microcrack Initiation and Propagation Beneath Hertzian Contacts in Polycrystalline Ceramics," *Acta Metall.*, **42** [5] 1683–93 (1994). □